Itinerant to localized electronic transition in $Sr_2FeMo_{1-x}W_xO_6$

R. I. Dass and J. B. Goodenough
Texas Materials Institute, ETC 9.102, University of Texas at Austin, Austin, Texas 78712-1063
(Received 8 August 2000; published 22 January 2001)

Structural, transport, and magnetic measurements on the system $Sr_2FeMo_{1-x}W_xO_6$ ($0 \leqslant x \leqslant 1$) have been used to monitor the transition from itinerant-electron ferromagnetism in Sr_2FeMoO_6 to localized-electron antiferromagnetism in Sr_2FeWO_6. An anomalous expansion of the cell volume with increasing x reflects the progressive localization of the minority-spin electrons. The percolation threshold for itinerant π^* electrons occurs in the interval $0.75 < x < 0.85$, and compositions in the range $0.8 < x < 1.0$ exhibit spin-glass behavior. For $x \leqslant 0.5$, antiferromagnetic coupling across antiphase boundaries produces an *M-H* hysteresis loop that, although having a low remanence and coercivity, nevertheless saturates by 10 kOe. A peculiar field dependence of the Weiss constant of the paramagnetic molar susceptibility disappears for $x \geqslant 0.25$. Transport and structural data are consistent with a relative stabilization of the d_{xy} π^* band relative to the $d_{yz \pm izx}$ π^* bands at lower temperatures and higher values of x.

DOI: 10.1103/PhysRevB.63.064417 PACS number(s): 75.30.Cr, 75.30.Et, 75.30.Kz, 71.30.+h

INTRODUCTION

Ordering of the Fe and Mo or W atoms on the octahedral *B* sites of the perovskite structure occurs in both Sr_2FeMoO_6 and Sr_2FeWO_6.[1–4] Sr_2FeWO_6 contains well-ordered Fe^{2+} and W^{6+} ions; it is an antiferromagnetic insulator with a localized high-spin configuration at the Fe^{2+} ions. Sr_2FeMoO_6, on the other hand, is a half-metallic ferri- or ferromagnet as a result of overlapping Fe^{3+}/Fe^{2+} and Mo^{6+}/Mo^{5+} redox couples.[5] The itinerant electrons occupy a minority-spin π^* band resulting from Fe-O-Mo interactions; the majority-spin electrons give a localized spin $S=5/2$ at the Fe atoms. In this compound, the saturation magnetization depends on the degree of order of the Fe and Mo atoms.[6,7] Moreover, the *M-H* curves exhibit little hysteresis, a feature that we have attributed to antiferromagnetic Fe-O-Fe interactions across antiphase boundaries.[8] We also observed a remarkable increase with applied magnetic field H in the paramagnetic Weiss constant from $\theta < T_c$ to $\theta > T_c$, which we interpreted to signal a shift of the itinerant-electron density away from the Mo toward the Fe atoms. However, this anomalous susceptibility may also be accounted for by a ferromagnetic impurity with a $T_c' > T_c$.[9] A candidate chemical inhomogeneity in disordered samples would be a layer of three (111) all-Fe planes rather than the double iron layer of an antiphase boundary.

Here we report measurements on the system $Sr_2FeMo_{1-x}W_xO_6$ ($0 \leqslant x \leqslant 1$) that were motivated by five questions concerning the evolution from itinerant to localized behavior of the minority-spin electrons: (1) Do the changes with x in the lattice parameters and cell volume reflect a larger cell volume for localized versus itinerant electrons as anticipated from the virial theorem? (2) How do the transport properties change with x and temperature T from electronic conduction in a π^* band to hole conduction via the Fe^{3+}/Fe^{2+} couple? (3) As the π^* band narrows with increasing x, is an increase in the orbital angular momentum of the minority-spin electrons reflected in the *M-H* hysteresis loop? (4) How does the field dependence of the paramagnetic molar susceptibility depend on x? and (5) what is the character of the *T-x* phase diagram?

While the work was in progress, Kobayashi *et al.*[10] published an investigation of the evolution with x of the magnetoresistance in the $Sr_2FeMo_{1-x}W_xO_6$ system. They reported (1) an increase with x in the degree of order of the *B*-site atoms, (2) the evolution of the *M-H* curves (not discussed) to obtain the magnetization $M_s(5\text{ K})$ versus x, (3) the variation of the resistivity $\rho(T)$ with x, but not of the thermoelectric power $\alpha(T)$, (4) the magnetic susceptibility of antiferromagnetic Sr_2FeWO_6, and (5) the change with x in the electronic specific heat. Our data are in essential agreement with theirs, but we did not obtain quite as high a degree of *B*-site order in our Mo-rich samples. Like them, we found a percolation threshold for metallic conduction and a spin-glass behavior beyond percolation ($x > 0.80$) where they found, at $x = 0.85$, a large, low-temperature negative magnetoresistance associated with inducing percolation of the ferromagnetic regions in a large H. They did not address the specific questions that motivated our study.

An early Mössbauer-spectroscopy study by Nakagawa *et al.*[11] was interpreted to reflect only Fe^{3+} for $x \leqslant 0.5$, both Fe^{3+} and Fe^{2+} at $x=0.7$, and only Fe^{2+} in Sr_2FeWO_6. However, the isomer shift for their ''Fe^{3+}'' ions is too high for that valence state[12] and would be better interpreted in an itinerant-electron model for the minority-spin electrons that give an effective iron valence $Fe^{2.6+}$. Indeed, Lindén *et al.*[13] have interpreted their recent Mössbauer data for $Sr_2FeMoO_{6-\delta}$ as indicating rapid (relative to 10^{-8} s) valence fluctuations with a mean valence $Fe^{2.5+}$. The early data are consistent with the minority-spin electrons remaining itinerant to $x=0.5$ with a progressive increase of localized Fe^{2+} configurations appearing in the range $0.50 < x \leqslant 0.70$ to coexist within a matrix containing itinerant minority-spin electrons.

EXPERIMENTAL PROCEDURES, RESULTS, AND DISCUSSION

A. Synthesis

Compounds of the system $Sr_2FeMo_{1-x}W_xO_6$ ($0 \leqslant x \leqslant 1$) were prepared from powders of $SrCO_3$, Fe_2O_3, MoO_3, and

TABLE I. The synthesis conditions and structural properties of the system $Sr_2FeMo_{1-x}W_xO_6(0\leqslant x\leqslant 1)$.

x	Synthesis conditions	a (Å)	c (Å)	$c/\sqrt{2}a$	V (Å^3)
0.00	1225 °C (0.1 h)	5.576(1)	7.904(1)	1.0023(3)	245.73(12)
0.00	1225 °C (0.1 h), 1250 °C (0.1 h)	5.576(1)	7.906(1)	1.0026(3)	245.81(12)
0.25	1275 C (8 h)	5.591(1)	7.891(1)	0.9980(3)	246.67(12)
0.50	1275 °C (8 h)	5.610(1)	7.901(1)	0.9959(3)	248.67(12)
0.75	1300 °C (18 h)	5.631(1)	7.917(2)	0.9942(4)	251.03(15)
0.78	1300 °C (40 h)	5.632(1)	7.919(1)	0.9942(3)	251.19(12)
0.79	1300 °C (40 h)	5.634(1)	7.921(1)	0.9941(3)	251.43(12)
0.80	1300 °C (40 h)	5.633(1)	7.925(1)	0.9948(3)	251.47(12)
0.85	1300 °C (24 h)	5.638(1)	7.932(1)	0.9948(3)	252.14(12)
0.87	1325 °C (36 h)	5.641(1)	7.931(1)	0.9942(3)	252.37(12)
0.88	1325 °C (38 h)	5.643(1)	7.936(1)	0.9944(3)	252.71(12)
0.89	1325 °C (38 h)	5.642(1)	7.934(1)	0.9944(3)	252.56(12)
0.90	1325 °C (48 h)	5.639(1)	7.935(1)	0.9950(3)	252.32(12)
0.91	1325 °C (100 h)	5.645(1)	7.940(1)	0.9946(3)	253.02(12)
0.94	1325 °C (124 h)	5.647(1)	7.942(1)	0.9945(3)	253.26(12)
0.95	1325 °C (76 h)	5.646(1)	7.943(1)	0.9948(3)	253.20(12)
0.96	1325 °C (148 h)	5.648(1)	7.942(1)	0.9943(3)	253.35(12)
0.97	1325 °C (124 h)	5.646(1)	7.944(1)	0.9949(3)	253.23(12)
0.98	1325 °C (148 h)	5.647(1)	7.945(2)	0.9949(4)	253.36(15)
1.00	1325 °C (76 h)	5.648(1)	7.942(2)	0.9943(4)	253.35(15)

WO_3 ground together in stoichiometric ratios and calcined at 900 °C in air for 3 h; the products were gray for $0\leqslant x\leqslant 0.5$ and red-brown for $0.5<x\leqslant 1.0$. These products were ground and pelletized into half-inch-diameter pellets 3 to 5 mm thick. The pellets were then annealed in a flowing mixture of 1% H_2/Ar at the temperatures and for the times indicated in Table I. All samples were then cooled in this atmosphere to room temperature at a rate of 180 °C/h; the pellets of the compositions $0\leqslant x\leqslant 0.75$ were blue-black in color while they were reddish-brown gray for $0.75<x\leqslant 1$.

B. Structure

The identification of all the phases and the determination of room-temperature lattice constants were accomplished with a Philips APD 3520 powder x-ray diffractometer and Cu $K\alpha$ radiation ($\lambda=1.54059$ Å); Mo was the internal standard. The data were collected in steps of 0.020° over the range $10°\leqslant 2\theta\leqslant 100°$. Lattice constants were refined by a least-squares method developed by Novak and Colville.[14] The lattice constants for the different compositions are found in Table I.

All samples were single-phase and exhibited a series of superstructure reflections due to ordering of the Fe and Mo/W atoms on the octahedral B sites of the perovskite structure. In this study, tetragonal crystal symmetry with space group $I4/mmm$ ($Z=2$) was observed for all compositions $0\leqslant x\leqslant 1$. As shown in Fig. 1, the a lattice parameter increases monotonically with x to $x\approx 0.92$ whereas the c parameter passes through a minimum near $x\approx 0.3$ and the axial ratio $c/\sqrt{2}a$ decreases from a value 1.0023 ± 0.0003 at $x=0$ to an almost constant value of 0.9945 ± 0.0004 for $x\geqslant 0.75$. The change of cell volume with x shows a sharp deviation from Végard's law that can be interpreted as a progressive change from itinerant to localized electronic behavior of the minority-spin electrons in the interval $0.3<x<0.93$, see Fig. 1(d). According to the virial theorem, which states

$$2\langle T\rangle+\langle V\rangle=0$$

for central-force fields, an increase in mean kinetic energy $\langle T\rangle$ as more minority-spin electrons become localized requires an increase in the magnitude $|\langle V\rangle|$ of the mean potential energy; for antibonding electrons, an increase in $|\langle V\rangle|$ is accomplished by an increase in the mean equilibrium Fe-O-Mo/W bond length. The tetragonal distortion is due to a cooperative rotation of the octahedral sites about an [001] axis; this distortion leads to an axial ratio $c/\sqrt{2}a>1$. Therefore, the decrease in $c/\sqrt{2}a$ with increasing x to a value less than unity must signal a lowering of the d_{xy} relative to the $d_{yz\pm izx}\,\pi^*$ states as would occur for a cooperative Jahn-Teller deformation at localized Fe^{2+} with high-spin configurations; in the paramagnetic phase, spin-orbit coupling would suppress a cooperative Jahn-Teller distortion of opposite sign that optimizes the orbital angular momentum. The minimum in the c versus x curve of Fig. 1(b) reflects the anomalous increase in cell volume with x for $x>0.3$.

The degree of B-site ordering on the octahedral sites was not determined by Rietveld refinement of the powder x-ray diffraction patterns. Instead, a qualitative estimate of B-site ordering was determined by observing the experimental relative intensity of the most intense superstructure reflection, which is the (101) reflection for $I4/mmm$. A monotonic increase in the relative intensity of this reflection with increasing x is consistent with the observation of Kobayashi *et al.*[10] of increasing order as x increases; the Coulomb forces responsible for order would be greater for W^{6+} and Fe^{2+} compared to $Mo^{(5+\delta)+}$ and $Fe^{(3-\delta)+}$.

C. Transport properties

Since resistivity measurements on polycrystalline samples contain a grain-boundary component whereas thermoelectric-power measurements reflect the intragrain properties, we measured the Seebeck coefficient $\alpha(T)$ for the entire solid-solution range, Fig. 2. The measurements were performed with a laboratory-built apparatus as described elsewhere.[15] Data for insulating samples such as Sr_2FeWO_6 became unreliable at low temperatures due to the impedance limits of the apparatus. A correction was applied to compensate for the small contribution to α from the copper leads.

The $x=0$ sample showed typical n-type metallic behavior with a linear temperature dependence. The metallic component remained dominant in the $x=0.25$ sample, but a transition from n-type to p-type conductivity was found at $T_{np}\approx 190$ K in the $x=0.50$ sample that cannot be attributed to a phonon drag enhancement; T_{np} increases with x and a crossover from n-type to p-type conduction at room temperature occurs in the range $0.80<x<0.85$. For $x\geqslant 0.85$, the conduc-

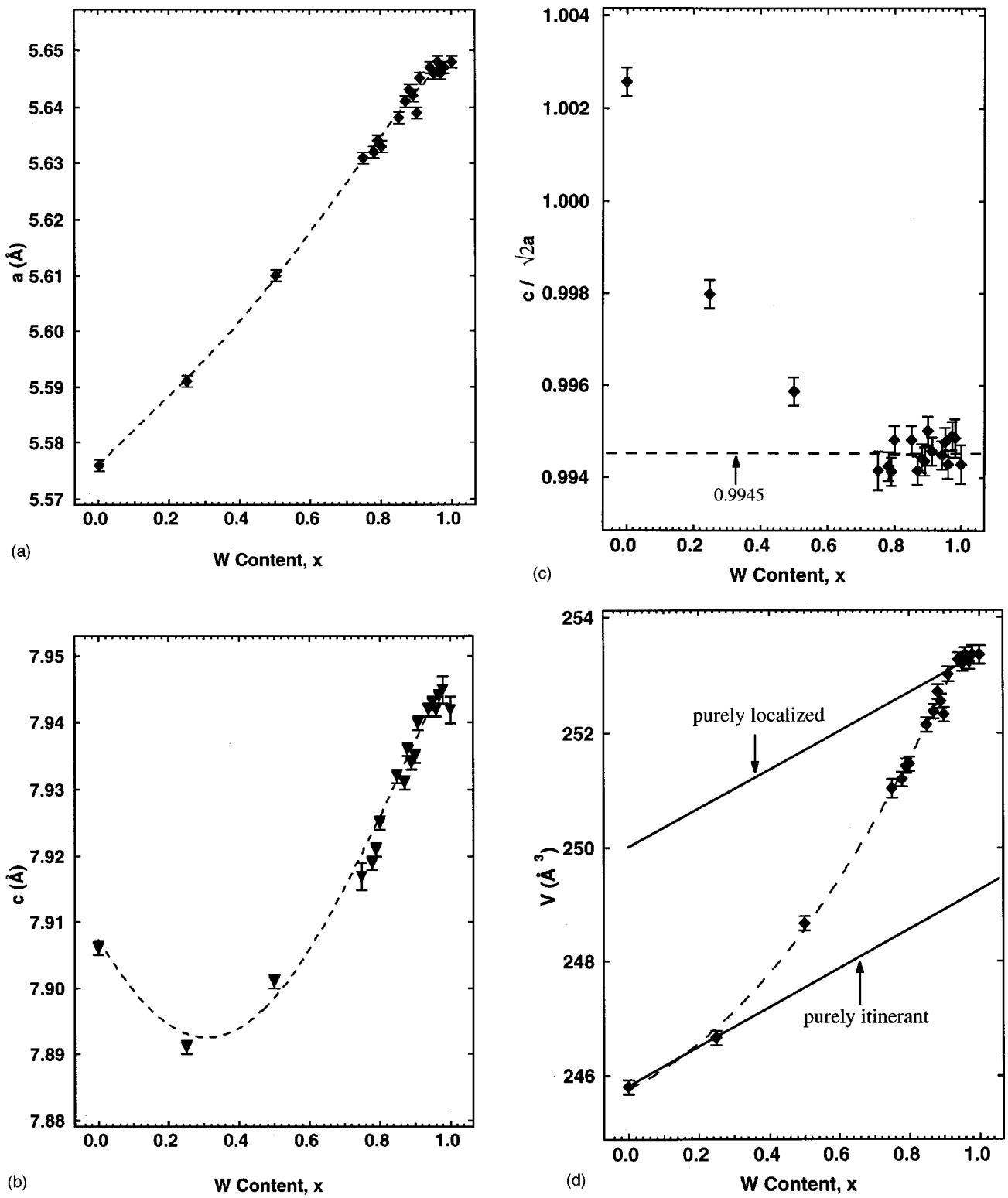

FIG. 1. The variation with W content x of (a) a, (b) c, (c) axial ratio $c/\sqrt{2a}$, and (d) cell volume V for the tetragonal system $Sr_2FeMo_{1-x}W_xO_6$.

tion is p-type at all temperatures; for $0.89 \leqslant x < 1.00$, a minimum in $\alpha(T)$ develops near 150 K that becomes sharper with increasing x.

To interpret these data, we consider the evolution of the π^* band states with increasing x. Perfectly ordered Sr_2FeMoO_6 would have threefold-degenerate minority-spin π^* bands one-sixth filled; therefore, we can expect n-type metallic behavior. The tungsten enters as W^{6+}, which removes x states per formula unit per π^* band and $(x-y)$ more are removed to form localized configurations at Fe^{2+}

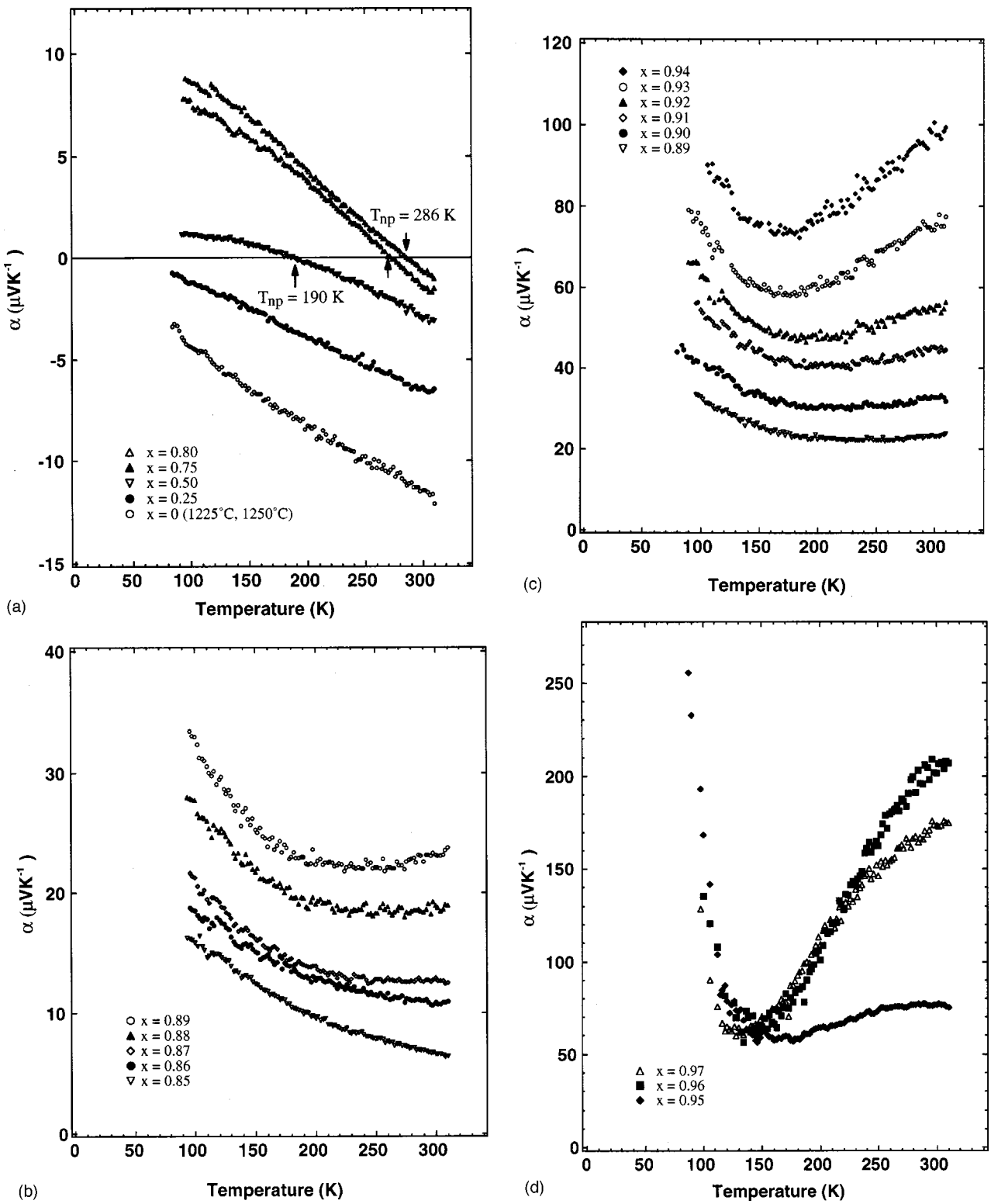

FIG. 2. The variation of the thermoelectric power $\alpha(T)$ for different x in the system $Sr_2FeMo_{1-x}W_xO_6$.

ions such that y decreases to zero as x increases to $x=1$. Stabilization of the minority-spin d_{xy} band relative to the $d_{yz\pm izx}$ bands would reduce the effective number of states in the conduction band to $(2-2x+y)$/formula unit whereas the number of electrons in the band would be $(1-y)$/formula unit. Conduction in the d_{xy} π^* band would become p-type for $(1-y)/(2-2x+y)>0.5$ or $x>1.5y$. Stabilization of the d_{xy} π^* band can be expected to increase with decreasing temperature as well as with decreasing bandwidth as x increases. Since the itinerant electrons would dominate $\alpha(T)$ so long as the percolation threshold for π^*-band formation is not exceeded, the evolution of the $\alpha(T)$ curves with increas-

ing x can be understood for $x<0.75$ from this qualitative argument. The change from metalliclike to semiconducting behavior in the range $0.75<x<0.85$, as also noted by Kobayashi *et al.*[10] from resistivity data, is consistent with a crossing of the percolation threshold for perovskites.

Beyond threshold for percolation of π^* -band states, i.e., for $x\geqslant 0.85$, the thermoelectric power becomes increasingly dominated by hole conduction on the Fe^{3+}/Fe^{2+} couple. At lower temperatures, the mobile holes are progressively trapped out. At higher temperatures, thermal excitation of electrons from trap states to Fe^{3+} appears to reduce the number of mobile charge carriers, particularly for $x>0.89$. At $x=0.85$, variable-range hopping between itinerant-electron clusters is probably the dominant conduction mechanism.

D. Magnetic data

Magnetic data were taken with a Quantum Design dc-SQUID magnetometer in the temperature range $5\,K\leqslant T\leqslant 700\,K$ and in applied magnetic fields from -50 kOe to 50 kOe. All samples in the range $0\leqslant x\leqslant 0.80$ had magnetization curves typical of a ferromagnet. The M-H curves taken at 5 K were similar to those reported by Kobayashi *et al.*[10] As shown in Fig. 3(a), the curves for $0\leqslant x\leqslant 0.50$ showed little hysteresis whereas the $x=0.75$ and 0.80 samples had hysteresis loops typical of that for a hard ferromagnet. Whereas saturation is achieved by 10 kOe for $x\leqslant 0.50$, it is not obtained even at 50 kOe for $x=0.75$ and 0.80, Fig. 3(b).

We[8] have attributed the low remanence M_r and coercivity H_{ci} in the $x=0$ sample to the presence of antiphase boundaries. Woodward *et al.*[16] have observed antiphase boundaries in two double-perovskite systems. Antiferromagnetic Fe-O-Fe interactions across an antiphase boundary would couple ferromagnetic regions on either side antiferromagnetically in low applied fields; but the ferromagnetic regions are large enough for the magnetic energy in 10 kOe to overcome the exchange energy across a boundary. Moreover, the orbital angular momentum of itinerant electrons is strongly suppressed, so the magnetocrystalline anisotropy is small. However, an increasing population of localized-electron Fe^{2+} configurations and the introduction of antiferromagnetic regions as x approaches the percolation threshold would introduce local anisotropies and make the M-H hysteresis loops appear more typical of a hard magnet that does not saturate even in a field of 50 kOe. For $x\geqslant 0.85$, where the ferromagnetic clusters do not percolate in zero magnetic field, M-H hysteresis loops at 5 K are still found, Fig. 4; they change smoothly into the anhysteretic straight line of the antiferromagnetic phase at $x=1.0$. The magnetic properties of the system at $T=5$ K are summarized in Table II.

Our magnetic susceptibility data for antiferromagnetic Sr_2FeWO_6 were identical to those given by Kobayashi *et al.*[10] Figure 5 shows the molar magnetic susceptibility $\chi_{mol}(T)$ in a magnetic field of 100 Oe (FC) or in zero field (ZFC) for samples $0.85\leqslant x\leqslant 0.95$. Before any measurements were made, the samples were heated to room temperature to remove any previous magnetic history. The data show spin-glass behavior typical of ferromagnetic clusters coupled through an antiferromagnetic matrix. The spin-freezing temperature T_f was taken as the maximum in the ZFC $\chi_{mol}(T)$ curves. A Curie temperature $T_c^*>T_f$ for the clusters decreases with the cluster size as x increases, as can be seen in the phase diagram of Fig. 6. An abrupt drop from $T_c\approx 400\,K$ for the percolating matrix to T_c^* for the isolated clusters occurs in the interval $0.75\leqslant x\leqslant 0.80$, Table III.

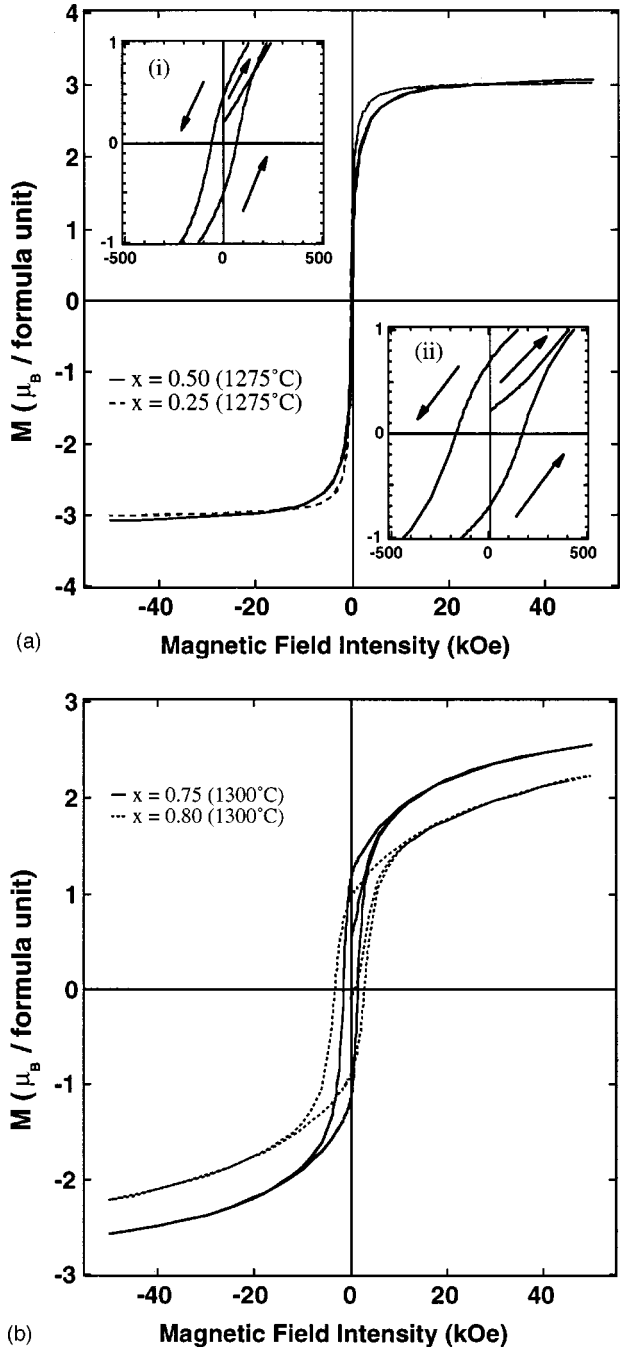

FIG. 3. The M-H hysteresis loops of the ferromagnetic compositions (a) $x=0.25$ and 0.50 and (b) $x=0.75$ and 0.80 of the system $Sr_2FeMo_{1-x}W_xO_6$ at $T=5$ K. Insets (i) and (ii) in (a) show the low coercivities and low remanences for $x=0.25$ and $x=0.50$, respectively.

Although saturation was achieved in the M-H loops for $x\leqslant 0.50$, the saturation magnetization increased with x to

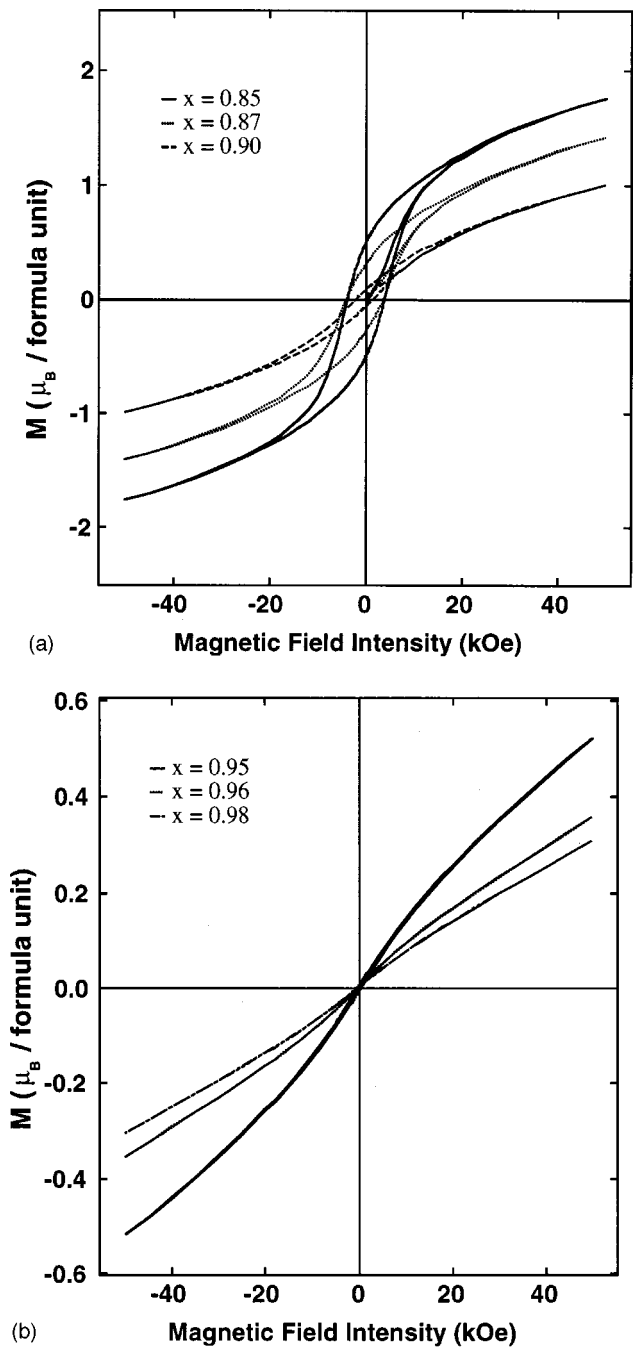

FIG. 4. The *M-H* hysteresis loops of different spin-glass compositions of $0.85 \leqslant x < 1.00$ in the system $Sr_2FeMo_{1-x}W_xO_6$ at $T = 5$ K.

only about $3.1\mu_B$/formula unit, significantly below the theoretical spin-only moment $M_s(0) = 4.0\mu_B$/formula unit for ideal *B*-site ordering. The *B*-site ordering clearly increased with x in this interval as was also found by Kobayashi *et al.*[10]

The field dependence of the paramagnetic inverse molar susceptibility $\chi_{\mathrm{mol}}^{-1}(T)$ of Sr_2FeMoO_6 is shown in Fig. 7 for $300\,\mathrm{K} \leqslant T \leqslant 700\,\mathrm{K}$. The Weiss constant θ is seen to shift, for $x = 0$, from $\theta < T_c$ to $\theta > T_c$. Since the magnetic energy for a shift of the density of minority-spin electrons from Mo to Fe is small compared to the bandwidth, this finding is quite remarkable. The magnitude of the effect implies, for a homogeneous system, a feedback mechanism that amplifies a shift in electron density. Such a feedback may reside in the sensitivity of the equilibrium Fe-O bond length to the degree of localization of the electrons via the virial theorem. However, it could only happen with overlapping redox energies and a bandwidth near the transition from localized to itinerant electronic behavior. This anomalous behavior is retained in the $Sr_{2-x}Ca_xFeMoO_6$ system, but it is suppressed by $x = 0.25$ in the $Sr_2FeMo_{1-x}W_xO_6$ system.

TABLE II. The magnetic properties of the system $Sr_2FeMo_{1-x}W_xO_6$ at $T = 5$ K. M(50 kOe), M_r, and H_{ci} are the magnetization at 50 kOe, the remanent magnetization, and the coercivity, respectively.

x	M(50 kOe) (μ_B/f.u.)	M_r (μ_B/f.u.)	H_{ci} (Oe)
0.00	2.69(2)	0.37	75(5)
0.25	3.02(2)	0.48	65(5)
0.50	3.09(2)	0.69	170(5)
0.75	2.57(2)	1.15	1460(5)
0.78	2.44(2)	1.07	2230(5)
0.79	2.33(2)	1.00	2740(5)
0.80	2.23(2)	0.92	3050(5)
0.85	1.76(2)	0.50	3890(5)
0.86	1.58(2)	0.38	3960(5)
0.87	1.42(2)	0.29	3900(5)
0.88	1.30(2)	0.20	3100(5)
0.90	1.00(2)	0.074	1830(5)
0.91	0.89(2)	0.046	1400(5)
0.92	0.80(2)	0.029	1040(5)
0.94	0.59(2)	0.010	550(5)
0.95	0.52(2)	0.005	340(5)
0.96	0.36(2)	0.001	90(5)
0.97	0.43(2)	0.003	260(5)
0.98	0.31(2)	0	60(5)
1.00	0.23(2)	0	15(5)

Alternatively, the anomalous character illustrated in Fig. 7 can be attributed to a chemical inhomogeneity (we found no evidence for an impurity phase) associated with the lack of ideal long-range order of the Fe and Mo atoms. If the chemical inhomogeneity introduces a local ferrimagnetic moment M' having a Curie temperature $T_c' > T_c$, then the measured molar susceptibility $\chi_{\mathrm{meas}} = \chi_{\mathrm{mol}} + (M'/H)$, where χ_{mol} is the intrinsic molar magnetic susceptibility. For a small M' and a large applied field H, (M'/H) is negligible compared to χ_{mol}, so a measurement in 50 kOe approaches the intrinsic χ_{mol}. In a lower field ($H = 2.5$ kOe), an $M' = 8.21$ emu/mol ($0.0015\mu_B$/formula unit) would add an (M'/H) term capable of giving χ_{meas} the character of the 2.5 kOe curve in Fig. 7. Measurement of M versus H at 600 K from 0 to 50 kOe and back gave a straight line that passed through zero within our experimental error, but an $M' \approx 0.0015\mu_B$/formula unit is at the limit of our resolution.

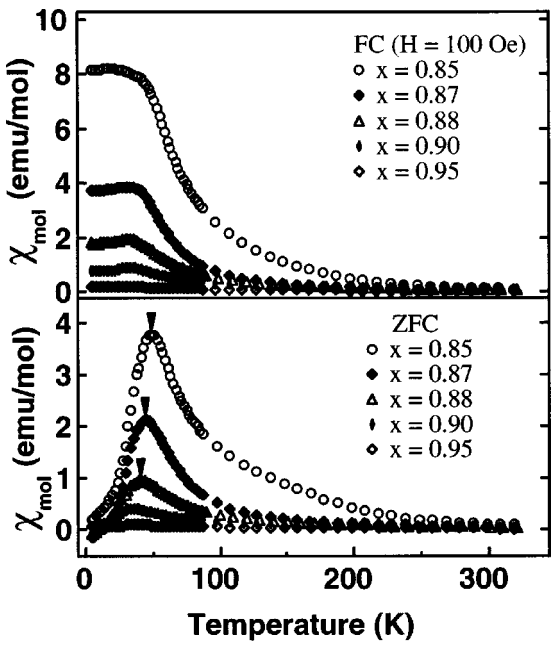

FIG. 5. The variation of the ZFC and FC ($H=100$ Oe) molar susceptibility $\chi_{mol}(T)$ for different compositions of $0.85 \leqslant x \leqslant 0.95$ in the system $Sr_2FeMo_{1-x}W_xO_6$. The spin-glass freezing transition is indicated for some of the compositions.

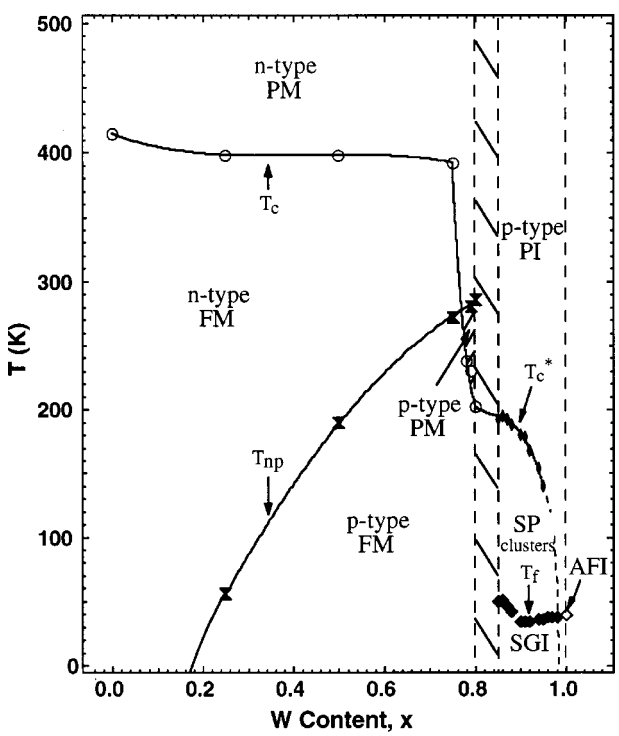

FIG. 6. The electronic and magnetic phase diagram of the tetragonal system $Sr_2FeMo_{1-x}W_xO_6$ ($0 \leqslant x \leqslant 1$). FM=ferromagnetic metal, PM=paramagnetic metal, PI=paramagnetic insulator, SP=superparamagnetic, SGI=spin-glass insulator, and AFI=antiferromagnetic insulator.

TABLE III. The type of magnetic behavior and magnetic transition temperatures of compositions in the system $Sr_2FeMo_{1-x}W_xO_6$($0 \leqslant x \leqslant 1$). F, SG, SP, and AF refer to ferromagnetism, spin glass, superparamagnetic clusters, and antiferromagnetism, respectively. T_f, T_c^*, T_c, and T_N are the spin-glass freezing temperature, the Curie temperature of ferromagnetic clusters, the Curie temperature of long-range ferromagnetic order, and the Néel temperature, respectively.

x	Type of magnetic behavior	T_r (K) (100 Oe)	T_C^* (K)	T_C (K)	T_N (K)
0.00	F			412(2)	
0.25	F			398(2)	
0.50	F			398(2)	
0.75	F			392(2)	
0.78	F			238(2)	
0.79	F			230(2)	
0.80	F			202(2)	
0.85	SG+SP	50(1)	192(2)		
0.86	SG+SP	51(1)	195(2)		
0.87	SG+SP	46(1)	192(2)		
0.88	SG+SP	42(1)	188(2)		
0.90	SG+SP	34(1)	180(2)		
0.91	SG+SP	34(1)	178(2)		
0.92	SG+SP	34(1)	168(2)		
0.94	SG+SP	36(1)	154(2)		
0.95	SG+SP	36(1)	140(2)		
0.96	SG	38(1)			
0.97	SG	38(1)			
0.98	SG	38(1)			
1.00	AF				39(1)

A candidate chemical inhomogeneity would be the following. At an antiphase boundary, two (111) all-Fe planes may be nearest neighbors; they would be negatively charged with respect to the local charge neutrality. The exchange of adjacent (111) Mo and Fe layers on one side would produce three (111) all-Fe planes; the added negative charge in the triple Fe layers would be more than compensated by a positive double all-Mo layer. Such an exchange would increase the electrostatic Madelung energy associated with the defect. Strong 180° Fe-O-Fe antiferromagnetic superexchange interactions between the three all-Fe layers ($LaFeO_3$ has a $T_N = 750$ K) would give a local ferrimagnetic moment M'. Such a chemical inhomogeneity would not show up as a structural second-phase impurity, but it could influence the paramagnetic susceptibility.

CONCLUSIONS

The five questions that motivated this work have been answered as follows.

(1) The transition from itinerant to localized minority-spin electrons produces an anomalous expansion with x of the cell volume as predicted from the virial theorem.

(2) The evolution of the thermoelectric power $\alpha(T)$ with

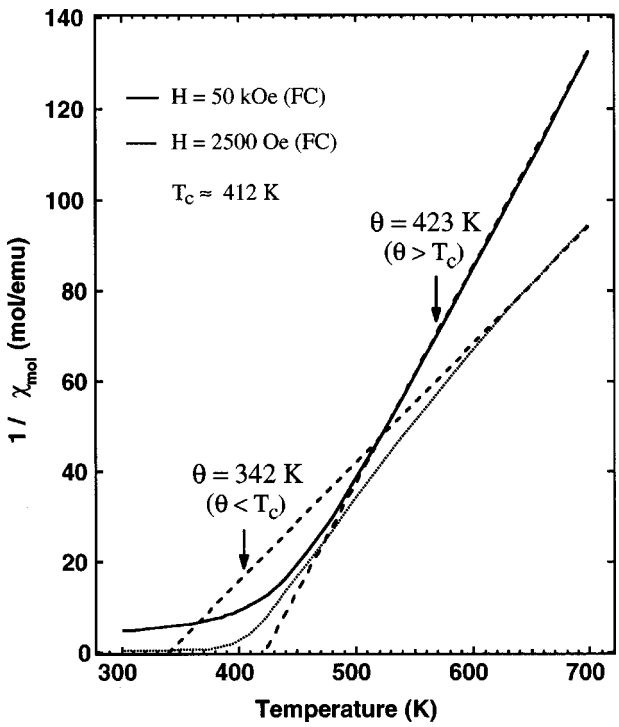

FIG. 7. The variation of the paramagnetic inverse molar susceptibility $\chi_{\mathrm{mol}}^{-1}(T)$ with temperature for Sr_2FeMoO_6 (1225 °C) in $H = 2500$ Oe and 50 kOe.

x shows a change from p-type to n-type with increasing temperature at a T_{np} that increases monotonically with x throughout the compositional range $0.2 \leqslant x \leqslant 0.75$ where the π^* electrons percolate through the structure. This change signals a stabilization of the d_{xy} π^* band relative to the $d_{yz\pm izx}$ π^* bands with decreasing temperature and as the band narrows with increasing x. This relative band stabilization also reduces the axial ratio $c/\sqrt{2}a$ to a value less than unity.

(3) For all $x \leqslant 0.5$, the M-H curves attain saturation by 10 kOe, but they exhibit low remanence M_r and coercivity H_{ci}. However, with the development of antiferromagnetic inclusions and localized Fe^{2+} configurations as x increases to the percolation threshold for itinerant π^* electrons, a strong anisotropy develops and saturation is not achieved by 50 kOe. The M-H curves evolve smoothly to that of an antiferromagnet only at $x = 1.0$, and a spin-glass freezing temperature T_f extrapolates smoothly to the Néel temperature $T_N \approx 39$ K of the $x = 1.0$ compound.

(4) The field dependence of the paramagnetic inverse molar susceptibility $\chi_{\mathrm{mol}}^{-1}(T)$ found at $x = 0$ is suppressed by $x = 0.25$, which contrasts with the $Sr_{2-x}Ca_xFeMoO_6$ system. This observation is consistent with a shift of the minority-spin electron density toward the Fe subarray with the introduction of W^{6+} near neighbors and with the Mössbauer data of Nakagawa *et al.*,[11] which showed an increase of 0.19 ± 0.05 mm/s in the isomer shifts between $x = 0$ and $x = 0.2$. If the anomalous paramagnetic susceptibility of Sr_2FeMoO_6 is due to chemical inhomogeneities, it may be suppressed by the greater degree of atomic order in the samples containing tungsten.

(5) The phase diagram of Fig. 6 shows retention of the ferromagnetic Curie temperature T_c near 400 K to $x = 0.75$ and spin-glass behavior for $0.8 < x < 1.0$, which indicates a percolation threshold for itinerant minority-spin electrons near $x = 0.80$. The spin-glass compositions exhibit p-type conductivity on the Fe^{3+}/Fe^{2+} couple of the matrix of localized-electron configurations; a change from n-type to p-type itinerant-electron conduction with increasing x and decreasing temperature can be interpreted as a relative stabilization of the d_{xy} relative to the $d_{yz\pm izx}$ π^* electrons. Only the $x = 1.0$ composition showed antiferromagnetic behavior with the spin-freezing temperature T_f of the spin-glass phase extrapolating appropriately to T_N of the $x = 1.0$ sample.

ACKNOWLEDGMENTS

The authors are grateful to the National Science Foundation and the Robert A. Welch Foundation of Houston, TX, for financial support.

[1] A. W. Sleight and R. Ward, J. Am. Chem. Soc. **83**, 1088 (1961).
[2] G. Blasse, Philips Res. Rep. **20**, 327 (1965).
[3] G. Blasse, J. Inorg. Nucl. Chem. **27**, 993 (1965).
[4] H. Kawanaka, I. Hase, S. Toyama, and Y. Nishihara, J. Phys. Soc. Jpn. **68**, 2890 (1999).
[5] A. W. Sleight and J. F. Weiher, J. Phys. Chem. Solids **33**, 679 (1972).
[6] K.-I. Kobayashi, T. Kimura, H. Sawada, K. Terakura, and Y. Tokura, Nature (London) **395**, 677 (1998).
[7] A. S. Ogale, S. B. Ogale, R. Ramesh, and T. Venkatesan, Appl. Phys. Lett. **75**, 537 (1999).
[8] J. B. Goodenough and R. I. Dass, Int. J. Inorg. Mat. **2**, 3 (2000).
[9] J. Fontcuberta is thanked for independently pointing this out.
[10] K.-I. Kobayashi, T. Okuda, Y. Tomioka, T. Kimura, and Y. Tokura, J. Magn. Magn. Mater. **218**, 17 (2000).
[11] T. Nakagawa, K. Yoshikawa, and S. Nomura, J. Phys. Soc. Jpn. **27**, 880 (1969).
[12] C. Gleitzer and J. B. Goodenough, Struct. Bonding (Berlin) **61**, 1 (1985).
[13] J. Lindén, T. Yamamoto, M. Karppinen, H. Yamauchi, and T. Pietari, Appl. Phys. Lett. **76**, 2925 (2000).
[14] G. A. Novak and A. A. Colville, Am. Mineral. **74**, 488 (1989).
[15] J. B. Goodenough, J.-S. Zhou, and J. Chan, Phys. Rev. B **47**, 5275 (1993).
[16] P. Woodward, R. D. Hoffmann, and A. W. Sleight, J. Mater. Res. **9**, 2118 (1994).